Sonic waveform attenuation in gas hydrate-bearing sediments from the Mallik 2L-38 research well, Mackenzie Delta, Canada

Gilles Guerin and David Goldberg

Borehole Research Group, Lamont-Doherty Earth Observatory, Palisades, New York, USA

Received 30 March 2001; revised 23 October 2001; accepted 28 October 2001; published 7 may 2002.

[1] The Japan Petroleum Exploration Co. Ltd./Japan National Oil Corporation/Geological Survey of Canada (JAPEX/JNOC/GSC) Mallik 2L-38 research well was drilled to 1150 m under the Mackenzie Delta, Canada, and penetrated a subpermafrost interval where methane hydrate occupies up to 80% of the pore space. A suite of high-quality downhole logs was acquired to measure in situ the physical properties of these hydrate-bearing sediments. Similar to other hydrate deposits, resistivity and compressional and shear sonic velocity data increase with higher hydrate saturation owing to electrical insulation of the pore space and stiffening of the sediment framework. In addition, sonic waveforms show strong amplitude losses of both compressional and shear waves in intervals where methane hydrate is observed. We use monopole and dipole waveforms to estimate compressional and shear attenuation. Comparing with hydrate saturation values derived from the resistivity log, we observe a linear increase in both attenuation measurements with increasing hydrate saturation, which is not intuitive for stiffening sediments. Numerical modeling of the waveforms allows us to reproduce the recorded waveforms and illustrate these results. We also use a model for wave propagation in frozen porous media to explain qualitatively the loss of sonic waveform amplitude in hydrate-bearing sediments. We suggest that this model can be improved and extended, allowing hydrate saturation to be quantified from attenuation measurements in similar environments and providing new insight into how hydrate and its sediment host interact.

INDEX TERMS: 0915 Exploration Geophysics: Downhole methods; 5144 Physical Properties of Rocks: Wave attenuation; 3210 Mathematical Geophysics: Modeling; 3025 Marine Geology and Geophysics: Marine seismics (0935); *KEYWORDS:* gas hydrate, sonic logging, attenuation, waveform modeling, frozen porous media

1. Introduction

[2] Gas hydrate is a crystalline compound made of water molecules arranged into ice cages that accommodate molecules of free gas. Its formation and stability in the subsurface are constrained by a relatively narrow range of high pressure and low temperature and depend on the influx of free gas [*Sloan*, 1990; *Kvenvolden*, 1994] and on the amount of gas dissolved in the pore fluid [*Buffett and Zatsepina*, 2000; *Xu and Ruppel*, 1999]. The ice-like structure causes strong changes in the physical properties of the host sediment, particularly mechanical properties, which makes it possible to infer their presence over wide areas in seismic surveys of various continental margins. In addition to deepwater sediments, conditions favorable for hydrate formation are also encountered in high-latitude sediments under deep permafrost. The Japan Petroleum Exploration Co. Ltd. (JAPEX)/Japan National Oil Corporation (JNOC)/Geological Survey of Canada (GSC) Mallik 2L-38 well was drilled in this type of environment (Figure 1), penetrating 1150 m of sands and sandstones interbedded with silt/clay layers, through a 640 meter thick permafrost [*Dallimore and Collett*, 1999].

[3] Downhole measurements, or logs, are used to measure continuously and in situ the physical properties of the formation surrounding a borehole. Because of the instability of hydrate at surface conditions, logs are critical to the evaluation of the in situ conditions conducive to hydrate formation. The measurements most sensitive to hydrate are resistivity, reacting to the insulating properties of ice and to the drilling-induced freshening of pore water, and the sonic log, which responds to the solidifying effect of solid ice in the pore space [*Collett*, 1998]. The logs collected in about 20 wells in the Mackenzie delta indicate that the local hydrate formation extends at least over 3600 km^2, with a thickness varying between 50 and 250 m [*Dallimore and Collett*, 1999].

[4] In this paper we summarize the main logs recorded in Mallik 2L-38 that identify clearly the hydrate-bearing intervals [*Collett et al.*, 1999a; *Lee and Collett*, 1999]. The analysis of the sonic waveforms recorded by the sonic probe shows that waveform amplitude is very low in the intervals were hydrate have been identified. We use the monopole and dipole waveforms to calculate the intrinsic sonic attenuation of the formation and use the hydrate saturation values derived from the resistivity log to establish a first empirical relationship between sonic attenuation and hydrate concentration. Numerical modeling of the sonic waveforms shows that sonic propagation in hydrates can be fully described with standard acoustic propagation models by changes in velocity and attenuation. As a preliminary qualitative explanation of our observations, we use a model for wave propagation in frozen porous media [*Leclaire et al.*, 1994] showing that sonic attenuation and velocity increase with hydrate saturation in hydrate-bearing sediments.

2. Logging Data

[5] Figure 2 shows some of the most significant logs recorded in the Mallik 2L-38 well. These logs were presented and described in detail by *Collett et al.* [1999a]. The caliper log in Figure 2a shows very little variation, which is an indicator of the high quality and reliability of most of the logs. The gamma ray and porosity logs (Figure 2b) show the limited variations in lithology and

0148-0227/02/2001JB000556$09.00

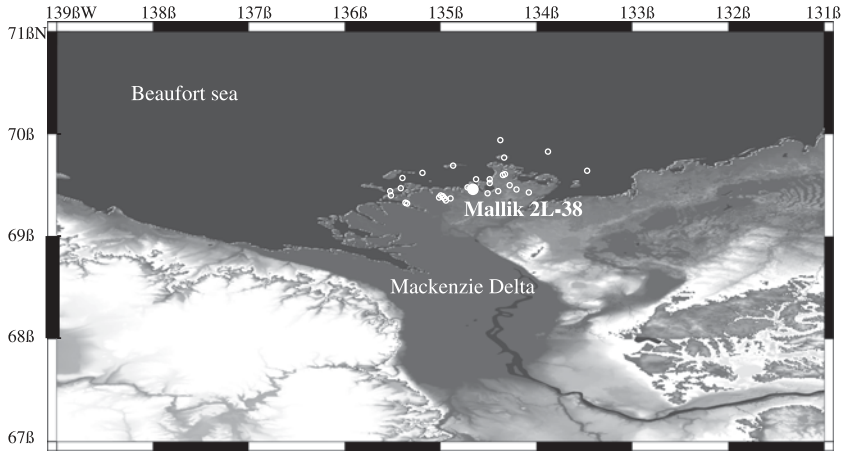

Figure 1. Location of the MALLIK 2L-38 Gas Hydrate Research Well in the Mackenzie Delta, Northwest Territories, Canada. Neighboring wells (hollow circles) were used by *Collett et al.* [1999b] to characterize the regional extent of the hydrate deposit.

porosity along the well. The presence of hydrate is indicated by higher resistivity and by higher compressional and shear velocity in Figures 2c, 2d, and 2e, respectively. This can be observed in particular over several intervals: 895–920, 950–995, 1005–1030, and 1070–1110 m (indicated by shaded areas). The relatively high gamma ray readings between these intervals (Figure 2b) indicate the presence of more shaly sediments and suggest a lithologic control on hydrate deposition: hydrate accumulates preferably in the larger pores of sandy intervals. The increase in shear velocity in hydrate-rich zones was observed in logging data by *Collett et al.*

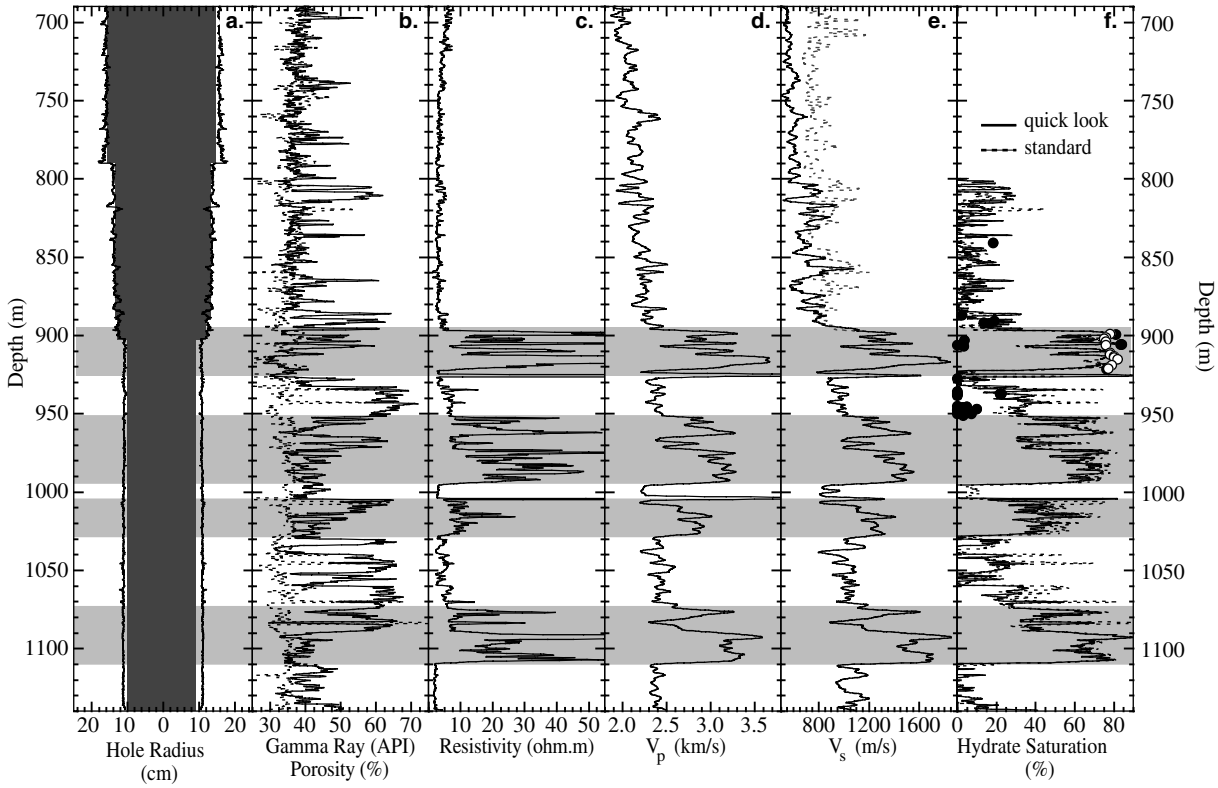

Figure 2. Downhole logs recorded in the Mallik 2L-38 well (data from *Collett et al.* [1999a]). Shaded areas indicate the presence of hydrate. (a) Caliper. The solid area represents the diameter of the drill bit. Bit changes occurred at ~790 and 900 m. (b) Lithology characterization for natural gamma ray (solid line) and porosity (dashed line). (c) Resistivity. (d) Compressional sonic velocity (V_p). (e) Shear sonic velocity (V_s). The dashed line shows the velocity log originally produced by automatic slowness-time coherence. The solid curve was reprocessed with an interactive semblance algorithm. (f) Gas hydrate concentration estimated from the resistivity log with the "quick look" and "standard" *Archie* [1942] relationships. Results of hydrate dissociation modeling (open circles) agree well, while chlorinity analysis (solid circles) suggests lower values.

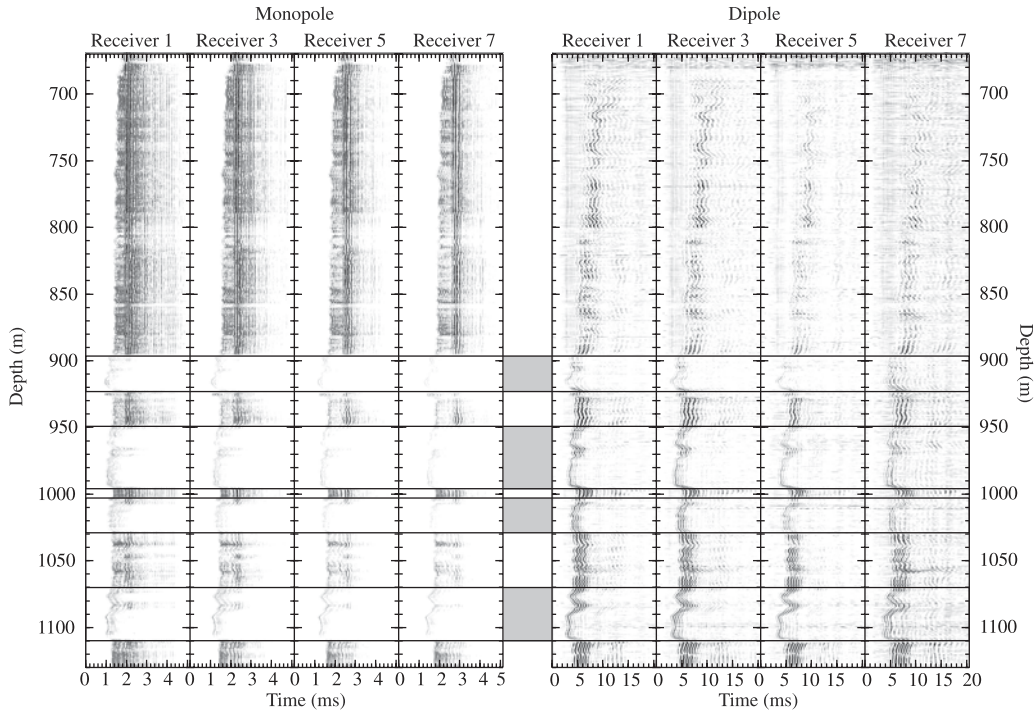

Figure 3. Sonic waveforms recorded with Schlumberger's dipole sonic imager tool. Only four out of the eight receivers are shown for each mode. Sampling rates are 100 and 25 kHz for monopole and dipole waveforms, respectively, with 512 samples per waveform. Intervals where hydrate have been identified in logs in Figure 2 are highlighted.

[1999a] and *Lee and Collett* [1999], and in the shear vertical seismic profile (VSP) data by *Sakai* [1999]. It is consistent with the results of the only previously recorded V_s log in hydrate-bearing sediments on the Blake Ridge [*Guerin et al.*, 1999].

[6] The V_s log in Figure 2e was reprocessed above ~900 m with an interactive semblance algorithm. The original V_s log computed at the time of the acquisition using an automatic slowness-time coherence (STC) procedure [*Kimball and Marzetta*, 1984] is shown for comparison. Above ~900 m, the automatic algorithm performed poorly, and *Sakai* [1999] noted a discrepancy between the V_s estimates of the shear VSP and of the original log above 840 m. The reprocessed V_s log agrees better with the VSP results. *Sakai* [1999] also notes that the V_s log has to be corrected for the dispersion of the flexural wave. *Harrisson et al.* [1990] show that the flexural dispersion bias does not exceed 10% at its strongest in very slow formations and very large boreholes. This is not a strong factor in these data. This reprocessed V_s log improves the accuracy of our attenuation estimation and the comparison between hydrate-bearing and hydrate-free sediments.

[7] *Lee and Collett* [1999] and *Collett et al.* [1999a] used both resistivity and sonic logs to estimate the amount of gas hydrate in the vicinity of Mallik 2L-38. They calculated saturation from the sonic velocity using weighted combination of the time-average and *Wood* [1941] formulations [*Lee and Collett*, 1999]. Their resistivity-derived estimates were calculated with *Archie*'s [1942] formulation. Both methods rely on time-honored models and agree overall on the hydrate concentration around the Mallik well. We use a "quick look" Archie method similar to the method described by *Collett* [1998] and *Guerin et al.* [1999] to calculate the hydrate saturation values in Figure 2f. In this method the resistivity data recorded in formations without hydrate are used as a baseline profile ($R_0(z)$) from which any increase is attributed to the presence of hydrate. The equation for the baseline in the Mallik well is calculated with a third-order polynomial fit to data in hydrate-free intervals (above 900 m and below 1120 m) and the saturation (S) is expressed in fraction of the pore space as a function of R_0 and of the recorded resistivity $R(z)$:

$$R_0(z) = 250 - 0.811z + 8.807 \times 10^{-4} z^2 - 3.162 \times 10^{-7} z^3 \quad (1)$$

$$S = 1 - [R_0(z)/R(z)]^{1/1.9386}, \quad (2)$$

where 1.19386 is an empirical constant determined by *Pearson et al.* [1983] and $R(z)$ is the deep resistivity recorded with the array induction tool (AIT). The gamma ray log shows that in the hydrate-bearing intervals the lithology is generally similar to the formation above 900 m, indicating that the baseline is a valid reference to estimate hydrate saturation in these intervals without correcting for lithology. The results (solid line) show that in intervals where the highest resistivity and sonic velocity are measured, hydrate saturation is close to 80%. For comparison, we show discrete saturation estimates from *Uchida et al.* [1999] calculated by chlorinity analysis of recovered core samples (solid circles) and results of hydrate dissociation modeling by *Wright et al.* [1999] (open circles). The dashed curve in the same track is the result of the "standard" Archie formulation described by *Collett et al.* [1999a]:

$$S = 1 - (aR_w/(R\Phi^m))^{1/1.9386}, \quad (3)$$

where a and m are empirical constants (*Collett et al.* [1999a; 1999b] use the so-called "Humble" values: $a = 0.62$ and $m = 2.15$) and R_w is the formation water resistivity, calculated with Arp's formula [*Desai and Moore*, 1969], using a linear regional temperature profile ($T(°C) = -23.1 + 0.036z$ [*Majorowicz and Smith*, 1999]) and a salinity of 25 ppt [*Collett et al.*, 1999a]. Figure 2f shows that the results of both standard and quick look Archie methods are similar, with maximum a maximum difference of the order of 10%. Because

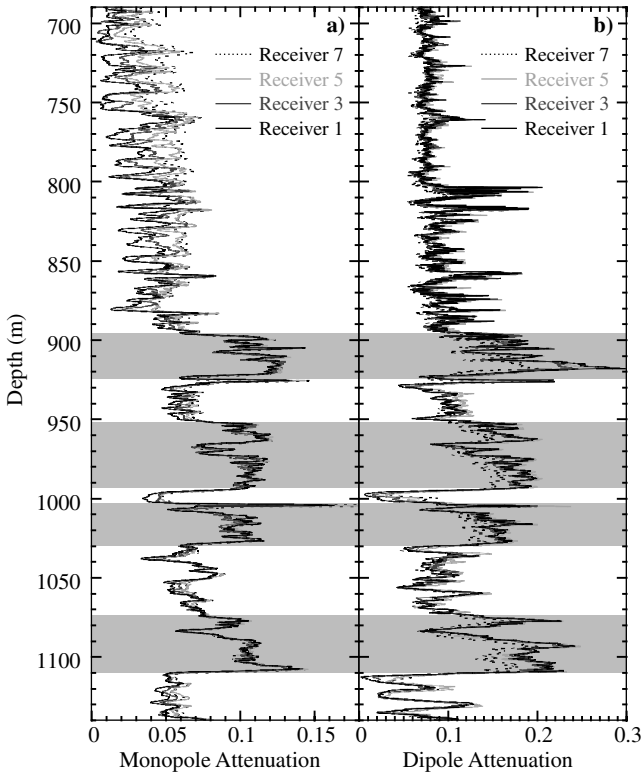

Figure 4. Attenuation logs calculated from the Mallik 2L-38 sonic waveforms using the method described by *Frazer et al.* [1997] and *Sun et al.* [2000]. (a) Monopole attenuation. (b) Dipole attenuation. Shaded areas indicate the main hydrate-bearing intervals.

it has slightly less scatter, we use the results of the quick look method for cross plots later in the paper.

3. Sonic Waveforms

[8] Sonic velocity logs are acquired by sending an acoustic pulse through the formation and recording it a known distance away with an array of receivers. Two kinds of sources are typically used: a monopole, which generates a spherical isotropic pressure pulse traveling at the compressional sound velocity, and a dipole, which produces an asymmetric pulse and flexural waves traveling near the shear velocity of the formation. The V_p and V_s logs in Figure 2 were calculated from, respectively, the monopole and dipole waveforms shown in Figure 3 by slowness-time coherence analysis [*Kimball and Marzetta*, 1984] and partially reprocessed by an interactive semblance algorithm. The reprocessed V_s log above 900 m accurately reflects the flexural mode arrival apparent with higher amplitudes in the dipole waveforms. All waveforms show distinctly earlier arrivals in intervals where hydrate are present, which corresponds to the velocity increase characteristic of hydrate. In addition, both types of waveform have significantly lower amplitudes in these intervals and the amplitude contrast between hydrate-bearing and hydrate-free intervals is stronger in the monopole waveforms.

4. Waveform Attenuation

[9] Waveform amplitude is the result of geometric (spherical) dispersion, tool coupling, and the intrinsic attenuation of the formation [*Goldberg et al.*, 1984]. Assuming that the energy emitted by the sonic transducer and the borehole shape are constant, geometric spreading and coupling are relatively uniform over the entire hole. Hence variations in waveform amplitude indicate a strong intrinsic attenuation in these hydrate-bearing sediments.

[10] Attenuation can be expressed as the loss of strain energy or wave amplitude in one cycle of waves oscillation. It is a function of frequency (f), or of the wave number ($\omega = 2\pi f$, the angular frequency), and is usually represented by the Q factor:

$$\frac{1}{Q(\omega)} = -\frac{1}{2\pi}\frac{\Delta E}{E} \tag{4a}$$

or

$$\frac{1}{Q(\omega)} = -\frac{1}{\pi}\frac{\Delta A}{A}, \tag{4b}$$

where ΔE and ΔA are the loss of energy and amplitude, respectively, during one cycle and E and A are the peak energy and maximum amplitude during the cycle. Q is usually considered independent of frequency over the limited range of frequency in logging tools [*Goldberg et al.*, 1984; *Paillet and Cheng*, 1991]. *Frazer et al.* [1997] and *Sun et al.* [2000] describe algorithms to derive in situ attenuation from full waveform logs. Applying a concept of "median frequency shift" to the amplitude spectrum of the recorded waveforms, *Sun et al.* [2000] derive a simple expression for the intrinsic attenuation of the formation:

$$Q^{-1}(z) = \frac{\left[A_i - \hat{\Phi}_i(z)\right]}{\Delta t_i(z)}, \tag{5}$$

where $\Delta t_i(z)$ is the travel time, $\hat{\Phi}_i(z)$ is calculated from the recorded waveforms and A_i is a constant characteristic of the source and of the tool geometry for each receiver. An expression for $\hat{\Phi}_i(z)$ is

$$\hat{\Phi}_i(z) \;=\; \text{median}_\omega\{\Phi(z,\omega) - \text{median}_z[\Phi(z,\omega) - \text{mean}_\omega\,\Phi(z,\omega)]\}, \tag{6}$$

where $\Phi(z, w) = 2 \ln X_i(z, \omega)/\omega$ and$X_i(z, \omega)$ is the power spectrum of the waveform recorded by the ith receiver. The subscripts indicate the variable on which the median or mean are calculated. The principle behind this expression is to average the spectrum over the frequency range to remove any depth-independent shift in the attenuation profile [*Frazer et al.*, 1997]. A first estimation of $Q^{-1}(z)$ can be calculated by choosing a reference value Q_{ref}^{-1} at a depth ξ, which will determine the values for A_i. Because it depends on an arbitrary reference, the resulting values represent the attenuation "relative" to this reference. If δ is the difference between the true attenuation at ξ and Q_{ref}^{-1} ($Q_{\text{true}}^{-1}(\xi) = Q_{\text{ref}}^{-1} - \delta$), and if we assume that the value of A_i is the same for all receivers, then δ can be calculated from the data at two receivers i and j:

$$\delta = \frac{(\Delta_i - \Delta_j)}{(\Delta t_i(\xi) - \Delta t_j(\xi))}$$

with

$$\Delta_i = \text{mean}_z[\;\hat{\Phi}_i(z) + Q_{\text{est}}^{-1}(z)\Delta t_i(z)]. \tag{7}$$

With this value of δ the true attenuation is

$$Q_{\text{true}}^{-1}(z) = Q_{\text{est}}^{-1}(z) - \delta\frac{\Delta t_i(\xi)}{\Delta t_i(z)}. \tag{8}$$

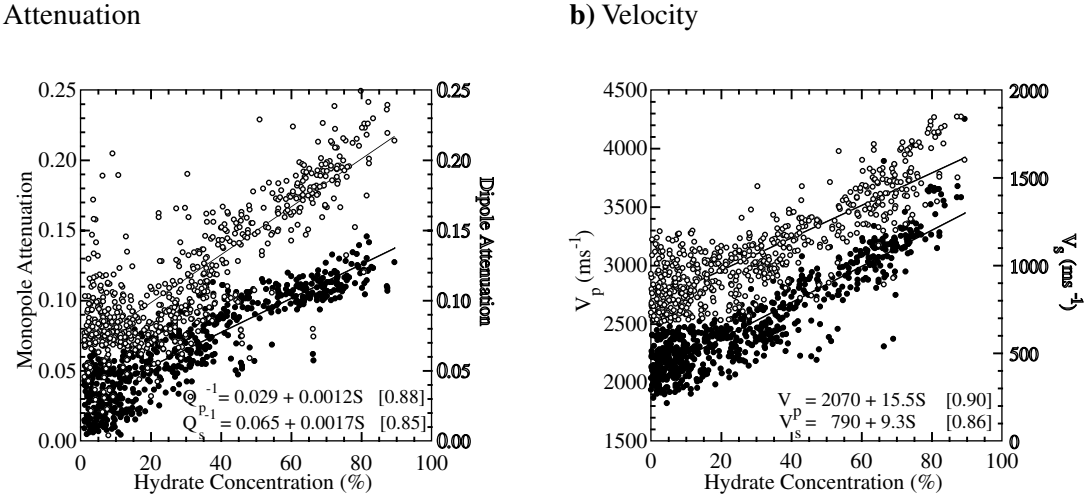

Figure 5. Relationship between gas hydrate saturation estimated from the resistivity log (quick look Archie) and (a) sonic attenuation and (b) sonic velocity. Solid circles are compressional values (Q_p^{-1} and V_p), open symbols are shear data (Q_s^{-1} and V_s). Regression coefficients for the least squares linear fits are in brackets.

The results of this procedure applied to the Mallik 2L-38 monopole and dipole waveforms are shown in Figures 4a and 4b, respectively. The results show that in the intervals where hydrate is present, the dipole attenuation increases by a factor of 2–3, and that monopole attenuation increases by almost 1 order of magnitude. For both monopole and dipole logs we display the results for receivers 1, 3, 5, and 7 to illustrate the consistency of the attenuation estimation between separate receivers.

[11] The correlation between attenuation and saturation is quantified by the cross plots shown in Figure 5a. In Figure 5b, we show a cross plot of V_p and V_s versus hydrate saturation. The least squares linear fit equations are

$$Q_p^{-1} = 0.029 + 0.0012S\ [0.88] \quad Q_s^{-1} = 0.065 + 0.0017S\ [0.85] \tag{9}$$

$$V_p = 2070 + 15.5S\ [0.90] \quad V_s = 790 + 9.3S\ [0.86], \tag{10}$$

where regression coefficients are in brackets.

[12] Despite a slightly wider scatter in the attenuation than in the velocity relationships, both Q_p^{-1} and Q_s^{-1} data sets have regression coefficients $\geq$0.84. The correlation quality for Q^{-1} likely differs from velocity correlations because of the differences in computational methods and because of the stronger sensitivity of attenuation to changes in formation physical properties. It is also due to the use of the velocity in calculating Q^{-1}, which includes the velocity uncertainty in the Q^{-1} calculations. Figure 5 shows, overall, that both attenuation and velocity can be related directly to hydrate saturation.

5. Waveform Modeling

[13] To understand how wave amplitudes relate to the physical properties of the formation, it is useful to model sonic waveforms while varying parameters such as sonic velocity and attenuation. We use the modeling technique described by *Tsang and Rader* [1979], *Cheng and Toksöz* [1981] and *Kurkjian and Chang* [1986]. Assuming that the borehole is an infinite fluid-filled cylinder in an infinite elastic medium, the excitation of a receiver located at a distance z from the transmitter is the sum of a direct pulse through the borehole fluid p_i and of a formation response pulse p_r given by

$$\begin{aligned} p_i &= \frac{1}{z}x\left(1-\frac{z}{V_f}\right) \\ p_r &= \frac{1}{(2\pi)^2}\int_{-\infty}^{\infty}\int_{-\infty}^{\infty}[X(\omega)A(k_z,\omega)]e^{ik_z z}e^{-i\omega t}dk_z\,d\omega, \end{aligned} \tag{11}$$

where $X(\omega)$ is the Fourier transform of the source pulse $x(t)$, V_f is the sonic velocity in the fluid, k_z is the along-axis wave number, and $A(k_z,\omega)$ a function describing the response of the formation [*Tsang and Rader*, 1979; *Kurkjian*, 1985; *Kurkjian and Chang*, 1986]. The attenuation is introduced by using complex velocities:

$$V \rightarrow V[\ 1 + 1n(\omega/\omega_0)/(\pi Q)](1 + j/2Q)^{-1}, \tag{12}$$

where ω_0 is the source central frequency and j is the unit imaginary complex number [*Cheng et al.*, 1982]. The source function is simplified by an exponentially decaying sinusoid. *Tsang and Rader* [1979] and *Kurkjian and Chang* [1986] use Hankel functions to give the expressions for A in the case of monopole and dipole source, respectively, and the branch cut integration is detailed by *Tsang and Rader* [1979] and *Kurkjian* [1985].

[14] Figure 6 shows the modeled waveforms corresponding to end-members values of V_p, V_s, Q_p^{-1}, and Q_s^{-1} in the different formations penetrated by the Mallik well. Only two receivers were simulated, the furthest corresponding to the middle (fifth) receiver in the array. Figures 6a and 6b show monopole and dipole waveforms, respectively. Each quadrant of four panels corresponds to fixed (V_p, V_s) with varying attenuation. In each quadrant, Q_p^{-1} increases from the left to the right panel and Q_s^{-1} from the top to the bottom panel. Generally, for a fixed combination of hole diameter, tool spacing and source frequency, the relative values of V_p, V_s, and V_f determine the different components observed in the waveforms such as compressional and shear head waves, trapped and surface modes [*Paillet and Cheng*, 1991]. Changing Q_p^{-1} and Q_s^{-1} values controls the amplitude of these

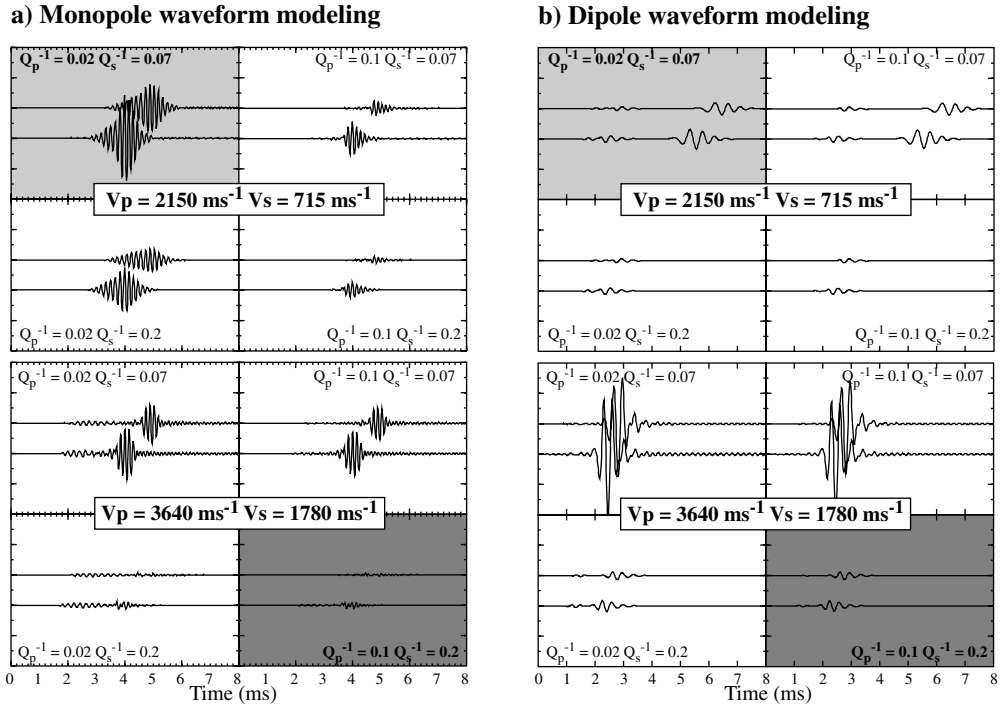

Figure 6. Results of waveform modeling for various velocity and attenuation values. (a) Monopole waveforms. (b) Dipole waveforms. Comparison between models and data have to include both monopole and dipole waveforms. Shaded panels correspond to values of Q^{-1} and V representative of Mallik 2L-38 with (dark) and without (light) hydrate.

modes. The entire set of model results shows that V_p, V_s, Q_p^{-1}, and Q_s^{-1} all influence the amplitude of the monopole waveforms, but dipole waveforms are mostly sensitive to V_s and Q_s^{-1}.

[15] By varying all the parameters and comparing simultaneously monopole and dipole waveforms with the recorded data, we evaluate various combinations of parameters to reproduce waveforms recorded at two depths in Mallik 2L-38 (Figure 7). For example, the dipole waveforms recorded at 800 m are reasonably well reproduced by the model with V_s = 715 m s^{-1} and Q_s^{-1} = 0.07 (Figure 6b, top panels). Comparison of the monopole waveforms

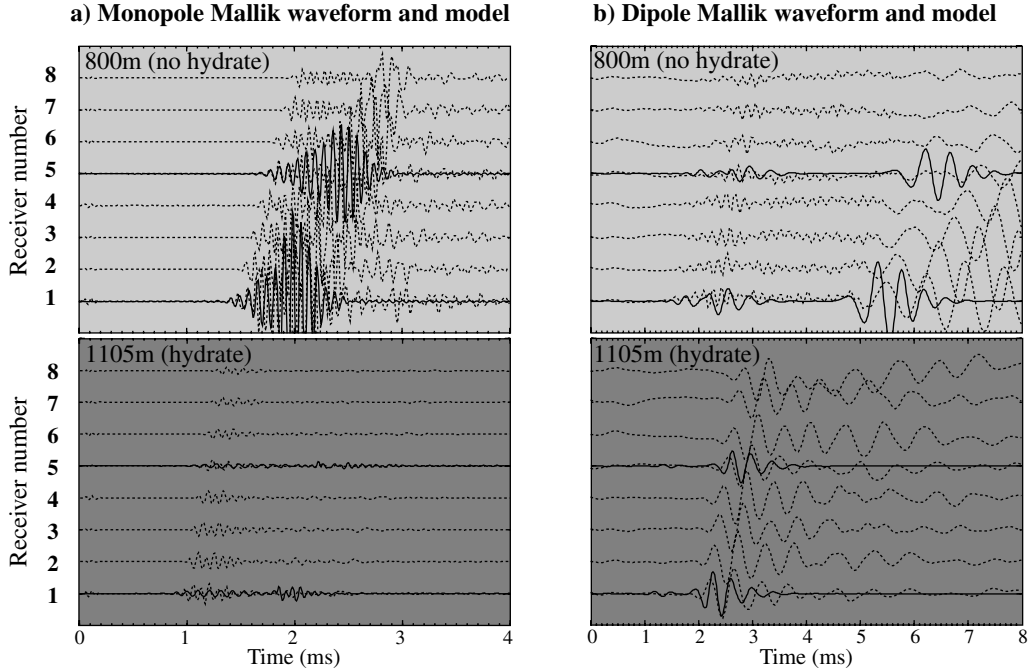

Figure 7. Comparison of recorded waveforms (dashed lines) with best matching models. The shading corresponds to the model with the same parameter values in Figure 6.

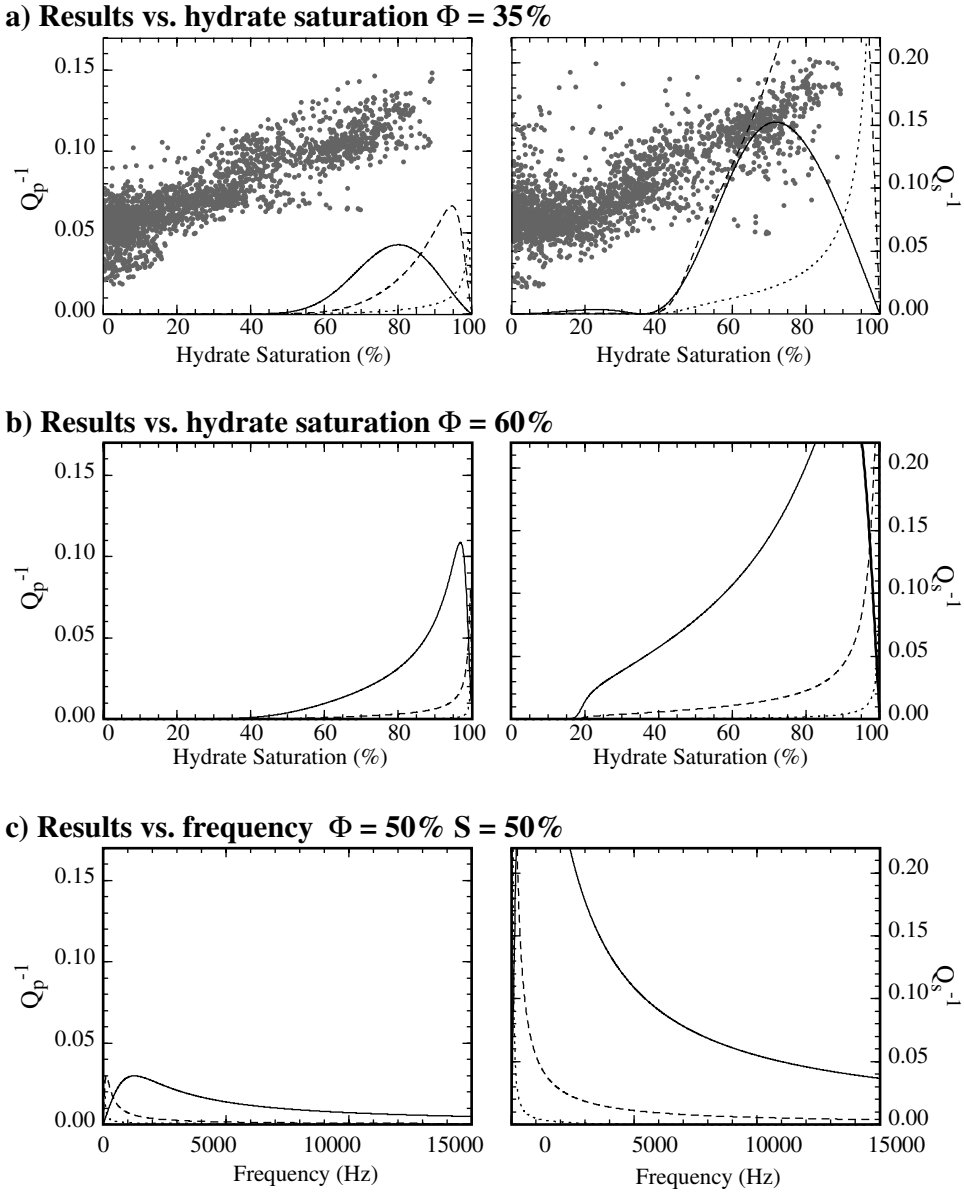

Figure 8. Predicted attenuation changes with hydrate saturation using the model of *Leclaire et al.* [1994] for wave propagation in frozen porous media. All models show results for three values of the ice permeability (dotted line is for $\kappa_{i0} = 10^{-8}$; dashed line is for $\kappa_{i0} = 10^{-9}$; and solid line is for $\kappa_{i0} = 10^{-10}$). (a) Results for a porosity of 35%, typical of the Mallik sediments. The data measured in the Mallik 2L-38 well are shown for comparison (same as Figure 5). (b) Results with a porosity of 60%, similar to the Blake Ridge. In Figures 8a and 8b, compressional frequency is 12 kHz and shear frequency is 2.5 kHz. (c) Results of the Leclaire et al. model as a function of frequency. Saturation and porosity are both 50%.

at the same depth, however, shows that the best match is obtained with $V_p = 2150$ m s^{-1} and $Q_p^{-1} = 0.02$ (Figure 6a, top left panel).

[16] The two sets of waveforms in Figure 7 (eight receivers for each mode) were recorded in the absence of and in the presence of hydrate, at 800 m and 1105 m, respectively . The results of the best matching models are superimposed for comparison. Despite wider frequency content and more noise in the recorded data than in the models, the synthetic waveforms reproduce the main features observed in the recorded data in both environments by varying only four parameters.

[17] Various components of the recorded waveforms can be identified by comparison with the models. At 800 m the first arrival in the short-offset monopole waveform (low amplitude at 1.5 ms) is the compressional wave followed by the fluid arrival (higher amplitude at ~1.8 ms). At this depth the shear velocity is much lower than V_f so there is no shear arrival. The compressional and fluid arrivals are also present in the dipole waveforms, although they have lower amplitudes than in the monopole waveforms. After 5 ms transit time the dipole waveform consists mostly of the flexural wave, but this mode appears to be more dispersive than predicted by the model. At 1105 m the monopole waveform at the short-offset receiver shows a compressional arrival at ~0.9 ms with a short- and low-amplitude tail. The fluid and shear waves arrive at 1.8 and 1.9 ms, respectively, and are very weak. At this depth the compressional arrival in the dipole waveforms is very weak at ~1 ms. The main component observed in the dipole waveforms is the flexural wave arrival at ~1.8 ms.

[18] These modeling results confirm that velocity and attenuation predictably influence sonic waveform shape and amplitude. An increase in Q^{-1} reduces the observed waveforms to essentially a single dominant component: a compressional mode for a monopole source and a flexural mode for a dipole source. Increase in Q^{-1} also suppresses later arrivals such as the shear and water arrivals in monopole waveforms and the slower components of the flexural mode in dipole waveforms. The presence or absence of hydrate in the formation, as shown at the two depths in Figure 7, can be modeled using conventional methods and reasonable parameterization of formation velocity (V_p and V_s) and attenuation (Q_p^{-1} and Q_s^{-1}).

6. Modeling of Frozen Porous Media

[19] Our waveform modeling shows that only four parameters may be used to simulate the observations and that these parameters (V_p, V_s, Q_p^{-1}, and Q_s^{-1}) can be extracted from sonic logs. We therefore considered models that could also predict these parameters in various fluid-solid media and found a preliminary suitable formulation developed by *Leclaire et al.* [1994]. They extend *Biot*'s [1956] theory of wave propagation to frozen porous media where ice particles and unfrozen water coexist. Assuming that the solid substrate and ice particle do not interact except in the case of a totally frozen medium, elastic waves propagate through a three-phase system: an effective solid grain matrix, the unfrozen water, and an effective solid ice matrix. Both matrices interact with the fluid but do not interact with each other. The longitudinal and transverse displacement potentials (φ and ψ) generated by the propagating waves are expressed by standard equations of propagation:

$$\mathbf{R}\,\nabla\varphi = \rho\ddot{\varphi} + \mathbf{A}\dot{\varphi} \qquad \text{and} \qquad \mu\nabla\psi = \rho\ddot{\psi} + \mathbf{A}\dot{\psi}, \tag{13}$$

where $\mathbf{R}$, μ, ρ, and $\mathbf{A}$ are the matrices of rigidity, shear moduli, mass densities, and friction coefficient, respectively, which are calculated with the properties of the effective media. Assuming that the wave has a single frequency ω, these equations can be solved by calculating the eigenvalues of $(\rho - j/\omega\mathbf{A})$ relatively to $\mathbf{R}$ and μ. This comes to calculating the complex roots ($\Lambda = \lambda_r + j\lambda_i$) of two polynomials for the compressional and shear waves, from where velocity and attenuation can be expressed by

$$V = 1/\lambda_r \qquad \alpha = 2V\lambda_i. \tag{14}$$

The coefficients of the different matrices are derived from various volumetric averages defined by the representation of each effective medium [*Kuster and Toksöz*, 1974; *Biot*, 1956]. Percolation theory is used to describe the transition of the system between continuous (fully saturated) and discontinuous (partially saturated) states. If we assume that hydrate can fill the entire pore space, the expressions for the bulk and shear modulus for the hydrate matrix are

$$K_{im} = K_{\max}S^{\tau} \qquad \mu_{im} = \mu_{\max}S^{\tau}, \tag{15}$$

where τ is a critical exponent estimated to be $\tau = 3.8$ [*Deptuck et al.*, 1985], $K_{\max}$ and $\mu_{\max}$ are maximum values of the elastic moduli estimated with the formulation of *Kuster and Toksöz* [1974], and S is the hydrate saturation. The model also uses explicit expressions for the permeability of both ice and grain matrices to calculate the energy dissipation and the attenuation in the friction coefficient matrix $\mathbf{A}$. The permeabilities are determined by Kozeny-Carman's relationships applied to the water fraction $\Phi(1 - S)$:

$$\kappa_s = \kappa_{s0}(1 - S)^3 \qquad \kappa_i = \kappa_{i0}S^{-2}[\Phi(1 - S)/(1 - \Phi)]^3, \tag{16}$$

where κ_{i0} and κ_{s0} are the permeabilities of the ice and grain matrices, respectively.

Table 1. Parameter Used in the Models

Parameter	Value
Grain density, kg m^{-3}	2,590
Water density, kg m^{-3}	1,000
Hydrate density, kg m^{-3}	900
Formation permeability, m^2	10^{-15}
Grain bulk modulus, $\times 10^9$ Pa	30
Grain shear modulus, $\times 10^9$ Pa	30
Water bulk modulus, $\times 10^9$ Pa	2.67
Hydrate bulk modulus, $\times 10^9$ Pa	6.4
Hydrate shear modulus, $\times 10^9$ Pa	15
Source frequency, Hz	12,000 (monopole) 2,500 (dipole)
Water viscosity, kg m^{-1} s^{-1}	1.8×10^{-3}

[20] Figure 8 shows some results of this model. The values used for the parameters are listed in Table 1. In Figure 8a we show the effect of hydrate saturation on attenuation for several values of κ_{i0}, which is the less constrained parameter, and for a porosity $\Phi = 35\%$, which is an average value in Mallik 2L-38. Our results calculated from the Mallik 2L-38 waveforms are also displayed. The best match between the measured data and the model is for $\kappa_{i0} = 10^{-10}$ m^2. The model curves do not reproduce the trends of the data, but they indicate increases in attenuation for increasing hydrate saturation. Both model and data also suggest that Q_s^{-1} is generally higher than Q_p^{-1} and that Q_s^{-1} starts to increase at lower hydrate saturations than Q_p^{-1}. The more rapid increase in Q_s^{-1} at low hydrate saturation may explain why only dipole waveforms are attenuated in the hydrate-bearing sediments of the Blake Ridge where saturation does not exceed 15% of the pore space [*Guerin et al.*, 1999]. In Figure 8b we display the result of the same model with $\Phi = 60\%$, typical of the Blake Ridge sediments. It shows that compressional attenuation does not become significant for saturations less than ~60%, while shear attenuation starts to increase with only 15% hydrate saturation, approximately the occupation of the pore space by hydrate the Blake Ridge.

7. Discussion

[21] While the presence of hydrate has been known to increase seismic velocity since the earliest investigations, only few studies of sonic waveform logs have been undertaken in hydrate-bearing sediments. Although the exact nature of the interaction between grains and hydrate is still subject to some debate, all observations and models agree that the occurrence of hydrate increases the compressional velocity of the formation [*Lee et al.*, 1996; *Ecker et al.*, 1998]. Fundamentally, the increase in V_p can be explained by the indurating effect of ice-like particles replacing water in open pore space. *Guerin et al.* [1999] observe similar increase in V_s logs in the hydrate-bearing sediments of the Blake Ridge, and the data from the Mallik 2L-38 well [*Collett et al.*, 1999a, 1999b; *Lee and Collett*, 1999] confirm conclusively that the presence of hydrate increases shear velocity. By comparison, waveform amplitude analyses in hydrate-bearing sediments are rare. *Guerin et al.* [1999] described the apparent attenuation of dipole waveforms in the sediments of the Blake Ridge but rough hole conditions and low hydrate concentration (<15% of the pore space) limited interpretation to a qualitative discussion. They observe dipole wave amplitudes to be lower in hydrates, but there is no apparent effect on monopole waveforms. The Mallik 2L-38 data suggest that given higher hydrate saturation, both monopole and dipole waveform amplitudes are affected by the presence of hydrate. To our knowledge, however, these sonic attenuation measurements in the Mallik 2L-38 well are the first quantitative attenuation estimates in hydrate-bearing sediments.

[22] In the Mallik 2L-38 well the velocity increase itself cannot explain the high attenuation in hydrate-bearing intervals: The strong positive correlation between attenuation and velocity that we observe in the Mallik 2L-38 well is not intuitive. In his review of sonic attenuation in marine sediments, *Hamilton* [1972] compiles data showing that attenuation decreases with decreasing porosity. If hydrate is considered as a pore-filling material, an increase in saturation corresponds to a decrease in porosity and, likewise, to a decrease in attenuation. *Goldberg et al.* [1984] calculated intrinsic attenuation from sonic waveforms in consolidated sediments but did not observe any correlation with velocity or porosity. *Goldberg et al.* [1985], however, describe an increase in attenuation with decreasing porosity and increasing velocity in marine sediments undergoing silica diagenesis. Because they are all made in different environments, these varying conclusions suggest that energy dissipation in sediments is controlled by smaller, pore-scale interactions between grains and infilling material, rather than by macroscopic bulk parameters such as velocity or porosity. Quantifying the relationship between attenuation and hydrate saturation may help to describe the grain-hydrate configuration at this microscopic scale. However, the physical mechanisms responsible for the increase in both velocity and attenuation in the presence of hydrate still remains to be determined. This mechanism may also be responsible for the blanking effect sometimes observed in seismic data that are associated with the presence of hydrate.

[23] Because attenuation is frequency-dependent, the energy dissipation in hydrate-bearing sediments does not necessarily translate from the sonic (1–20 kHz) to the seismic frequency range (1–200 Hz). *Wood et al.* [2000] used spectral inversion of single-channel seismic and VSP data to calculate *P* wave seismic attenuation on the Blake Ridge. They observe slightly higher attenuation values in the hydrate-bearing intervals but conclude that attenuation is likely not responsible for the observed seismic blanking. They also note, however, that attenuation may be affected by hydrate at shorter wavelengths and with higher concentrations. *Wood and Ruppel* [2000] argue that the reduced reflectivity on the Blake Ridge is due to scattering and destructive interference rather than to the homogeneity of the formation, as suggested by *Holbrook et al.* [1996]. If attenuation and scattering above the bottom simulating reflector (BSR) were high enough, this strong reflector might likewise be attenuated. This is not the case on the Blake Ridge. The impedance contrast across the BSR is so large that the attenuation above would have to be unrealistically high in order to reduce this reflector significantly. To reduce its amplitude by one order of magnitude over a hydrated thickness of ~0.2 ms two-way travel time (twtt), equation (4) shows that Q^{-1} should be on the order of 5×10^{-2} at ~100 Hz. *Wood et al.* [2000] estimate seismic attenuation to be ~5–10 times less within the hydrate stability zone. Therefore the BSR persists despite seismic scattering and attenuation above it. Low seismic amplitudes in the hydrate-bearing interval above this BSR is most likely a combination of different mechanisms, including intrinsic attenuation within hydrate, seismic scattering at bed boundaries and lithologic uniformity.

[24] In the Mackenzie delta the high hydrate concentrations should affect seismic amplitude, in a similar and complex manner. In the two-dimensional seismic lines presented by *Collett et al.* [1999b], no attenuation is apparent in hydrate-bearing intervals (~700–900 ms twtt). However, alternating hydrate-bearing and hydrate-free intervals that reflect seismic energy may be too thin (less than a seismic wavelength) to resolve seismic amplitude loss within the hydrate intervals alone. The compressional wave VSP described by *Sakai* [1999] and *Walia et al.* [1999] do not show high apparent attenuation either, although *Sakai* [1999] notes that the shear VSP may be strongly attenuated between 950 and 1000 m depth. This interval contains the bulk of the hydrate deposit in Mallik 2L-38. Although it is not entirely clear how hydrate attenuates seismic waves, nor which other formation effects may or may not be present, these results suggest that the effect of hydrate on the attenuation of shear waves is stronger than on compressional waves.

[25] Despite the present limitations of this model, we have also used the *Leclaire et al.* [1994] model to predict the influence of frequency on attenuation due to the presence of hydrate in porous sediments. In Figure 8c we show the results for three values of the ice permeability κ_{i0} and over a frequency range from seismic to sonic logging experiments (0.1 Hz to 15 kHz). We use values of porosity and saturation of 50%, between the end-member values on the Blake Ridge and in the Mackenzie delta. For $\kappa_{i0} = 10^{-10}$, which seems to give the most realistic values, compressional attenuation increases with frequency to ~1 kHz then decreases steadily to 15 Hz but remains low. By contrast, shear attenuation is high at frequencies below 1 kHz and decreases rapidly while remaining significant at least for $\kappa_{i0} = 10^{-10}$. Q_s^{-1} decreases more gradually as ice permeability κ_{i0} decreases. These results are consistent with the observed shear attenuation in hydrate-bearing intervals for logging and VSP experiments.

[26] In general, the *Leclaire et al.* [1994] model predicts lower attenuation and velocity than we observe in the Mallik 2L-38 well. The difference between the model and our data tends to decrease with increasing hydrate saturation. Our observations indicate an increase in velocity and attenuation at very low hydrate saturation, while the model predicts a significant increase only at saturations greater than ~40%. This may result from the assumption that ice/hydrate and grains do not interact. Only interactions between ice and fluid, and separately between fluid and grains, are allowed in the model for numerical simplicity. As a result, interaction between grains and hydrate occurs indirectly through the pore fluid and does not become significant until a critically high hydrate saturation level. Certain forms of hydrate deposition, such as uniform distribution of hydrate on grain surfaces, may also generate dissipative frictional interaction between grains and hydrate which should introduce more attenuation at lower saturations than predicted by this model. Despite its limitations, the Leclaire model offers a qualitative approach that explains our observations: high compressional and shear wave attenuation as well as an increase in attenuation with increasing hydrate saturation in the Mallik 2L-38 well.

[27] As an alternative or compounding explanation, the observed attenuation in these hydrate-bearing sediments may be enhanced by the presence of free gas, which is not considered in this model. Low concentrations (<20%) of free gas can increase sonic attenuation significantly [*Murphy*, 1982]. At high hydrate saturation such as in the Mackenzie delta sediments, there could be two main reasons for the presence of free gas: (1) pore water content may be insufficient for complete methane hydration, and some free gas remains in the pore space and (2) drilling operations may have induced dissociation of hydrate in the vicinity of the borehole. Such partial dissociation effects and the resulting influence of free gas on the observed sonic waveforms are difficult to quantify. However, anticipating these effects, the temperature of the drilling mud was reduced during drilling operations in order to limit hydrate decomposition [*Ohara et al.*, 1999]. Though motivated by safety reasons, this measure should have limited the physical extent of hydrate dissociation to the immediate vicinity of the borehole and any liberated free gas should have been evacuated by the drilling fluids before logging. In either case, any remaining amount of free gas should significantly reduce the compressional velocity. The sonic log measures high V_p in the hydrate-bearing intervals, and therefore the amount of free gas is extremely limited. We conclude that free gas should contribute only modestly, if at all, to the observed waveforms attenuation.

[28] A principal result of this study is the quantitative relationships established between attenuation and saturation. Equations (9) and (10) provide empirical tools that can be used to relate

attenuation to hydrate content in the Mackenzie delta sediments. High attenuation observed in the Mallik 2L-38 well supports qualitative observations made previously on the Blake Ridge under less favorable conditions. It now seems clear that amplitude losses in sonic logs, similar to low amplitudes commonly observed in seismic data, can be associated with the presence of hydrate and may help to quantify hydrocarbon concentrations. However, it will be necessary to develop new models or modify the Leclaire model to better reconcile analytic results with field observations before the physical mechanisms of attenuation in hydrate are fully understood. Future developments will need to account for the hydrate-grain interaction in three-phases systems and to consider the potential coexistence of free gas.

8. Conclusion

[29] We have quantified the attenuation, both Q_p^{-1} and Q_s^{-1}, from sonic waveforms recorded in hydrate-bearing sediments for the first time. Numerical modeling of the Mallik 2L-38 waveforms illustrates the influence of hydrate on the elastic properties of the formation, which can be parameterized using conventional expressions for borehole wave propagation. The increase in attenuation with increasing hydrate concentration in the Mackenzie delta sediments can be approximated to the first order by linear relationships: $Q_p^{-1} = 0.029 + 0.12S$, and $Q_s^{-1} = 0.065 + 0.17S$. The results of a poroelastic model for wave propagation in frozen porous media, including a percolation theory approach to describe energy dissipation, provide a preliminary qualitative explanation for these observations. The precise nature of the hydrate-grain interaction and the presence of free gas in this model, however, need to be further developed.

[30] **Acknowledgments.** The well logging data used in this study were collected as part of the scientific program for the JAPEX/JNOC/GSC Mallik 2L-38 Gas Hydrate Research Well. We are grateful to Scott Dallimore, Takashi Uchida, and Tim Collett for giving us the opportunity to work on this unique data set. The comments by I. Pecher, R. Hyndmann, and an anonymous editor were very valuable and improved the quality of this paper.

References

Archie, G. E., The electrical resistivity log as an aid in determining some reservoir characteristics, *J. Pet. Technol.*, *5*, 1–8, 1942.

Biot, M. A., Theory of propagation of elastic waves in a fluid saturated porous solid, *J. Acoust. Soc. Am.*, *28*, 168–191, 1956.

Buffett, B. A., and O. Y. Zatsepina, Formation of gas hydrate from dissolved gas in natural porous media, *Mar. Geol.*, *164*, 69–77, 2000.

Cheng, C. H., and M. N. Toksöz, Elastic wave propagation in a fluid-filled borehole and synthetic acoustic logs, *Geophysics*, *46*, 1042–1053, 1981.

Cheng, C. H., M. N. Toksöz, and M. E. Willis, Determination of in situ attenuation from full waveform acoustic logs, *J. Geophys. Res.*, *87*, 5477–5484, 1982.

Collett, T. S., Well log evaluation of gas hydrate saturations, *Trans. SPWLA Ann. Logging Symp.*, *39th*, paper MM, 1998.

Collett, T. S., R. E. Lewis, S. R. Dallimore, M. W. Lee, T. H. Mroz, and T. Uchida, Detailed evaluation of gas hydrate reservoir properties using JAPEX/JNOC/GSC Mallik 2L-38 gas hydrate research well downhole well log displays, in *Scientific Results from JAPEX/JNOC/GSC Mallik 2L-38 Gas Hydrate Research Well, Mackenzie Delta, Northwest Territories, Canada*, edited by S. R. Dallimore, T. Uchida, and T. S. Collett, *Bull. Geol. Surv. Can.*, *544*, 295–312, 1999a.

Collett, T. S., M. W. Lee, S. R. Dallimore, and W. F. Agena, Seismic- and well-log-inferred gas hydrate accumulations on Richards Island, in *Scientific Results from JAPEX/JNOC/GSC Mallik 2L-38 Gas Hydrate Research Well, Mackenzie Delta, Northwest Territories, Canada*, edited by S. R. Dallimore, T. Uchida, and T. S. Collett, *Bull. Geol. Surv. Can.*, *544*, 357–376, 1999b.

Dallimore, S. R., and T. S. Collett, Regional gas hydrate occurrences, permafrost conditions, and Cenozoic geology, Mackenzie Delta area, in *Scientific Results from JAPEX/JNOC/GSC Mallik 2L-38 Gas Hydrate Research Well, Mackenzie Delta, Northwest Territories, Canada*, edited by S. R. Dallimore, T. Uchida, and T. S. Collett, *Bull. Geol. Surv. Can.*, *544*, 31–44, 1999.

Deptuck, D., J. P. Harrison, and P. Zawadski, Measurement of elasticity and conductivity of a three-dimensional percolation system, *Phys. Rev. Lett.*, *54*(9), 913–916, 1985.

Desai, K. P., and E. J. Moore, Equivalent NaCl concentrations from ionic concentrations, *Log Anal.*, *10*(3), 12–21, 1969.

Ecker, C., J. Dvorkin, and A. Nur, Sediments with gas hydrates: Internal structure from seismic AVO, *Geophysics*, *63*, 1659–1669, 1998.

Frazer, L. N., X. Sun, and R. H. Wilkens, Changes in attenuation with depth in an ocean carbonate section: ODP sites 806 and 807, Ontong Java plateau, *J. Geophys. Res.*, *102*, 2983–2997, 1997.

Goldberg, D., T. K. Kan and J. P. Castagna, Attenuation measurements from sonic log waveforms, *Trans. SPWLA Annu. Logging Symp.*, *25th*, paper N, 1984.

Goldberg, D., D. Moos, and R. N. Anderson, Attenuation change due to diagenesis in marine sediments, *Trans. SPWLA Annu. Logging Symp.*, *26th*, paper KK, 1985.

Guerin, G., D. Goldberg, and A. Meltser, Characterization of in situ elastic properties of gas hydrate-bearing sediments on the Blake Ridge, *J. Geophys. Res.*, *104*, 17,781–17,796, 1999.

Hamilton, E. L., Compressional-wave attenuation in marine sediments, *Geophysics*, *37*, 620–646, 1972.

Harrisson, A. R., C. J. Randall, J. B. Aron, C. F. Morris, A. H. Wignall, R. A. Dworak, L. L. Rutledge, and J. L. Perkins, Acquisition and analysis of sonic waveforms from a borehole monopole and dipole source for the determination of compressional and shear speeds and their relation to rock mechanical properties and surface seismic data, paper SPE 20557 presented at the 65th Annual Technical Conference and Exhibition, Soc. of Pet. Eng., New Orleans, La., 1990.

Holbrook, W. S., H. Hoskins, W. T. Wood, R. A. Stephen, and D. Lizarralde, and Leg 164 Science Party, Methane hydrate and free gas on the Blake Ridge from vertical seismic profiling, *Science*, *273*, 1840–1843, 1996.

Kimball, C. V., and T. L. Marzetta, Semblance processing of borehole acoustic array data, *Geophysics*, *49*, 274–281, 1984.

Kurkjian, A. L., Numerical computation of individual far-field arrivals excited by an acoustic source in a borehole, *Geophysics*, *50*, 852–866, 1985.

Kurkjian, A. L., and S. K. Chang, Acoustic multipole sources in fluid-filled boreholes, *Geophysics*, *51*, 148–163, 1986.

Kuster, G. T., and M. N. Toksöz, Velocity and attenuation of seismic waves in two-phase media, 1, *Theoretical formulation, Geophysics*, *39*, 587–606, 1974.

Kvenvolden, K. A., Natural gas hydrate occurrence and issues, in *International Conference on Natural Gas Hydrates*, edited by E. D. Sloan, J. Happel, and M. A. Hnatow, *Ann. N. Y. Acad. Sci.*, *715*, 232–246, 1994.

Leclaire, P., F. Cohen-Tenoudji, and J. Aguirre-Puente, Extension of Biot's theory of wave propagation to frozen porous media, *J. Acoust. Soc. Am.*, *96*, 3753–3768, 1994.

Lee, M. W., and T. S. Collett, Amount of gas hydrate estimated from compressional and shear wave velocities at the JAPEX/JNOC/GSC Mallik 2L-38 gas hydrate research well, in *Scientific Results from JAPEX/JNOC/GSC Mallik 2L-38 Gas Hydrate Research Well, Mackenzie Delta, Northwest Territories, Canada*, edited by S. R. Dallimore, T. Uchida, and T. S. Collett, *Bull. Geol. Surv. Can.*, *544*, 313–322, 1999.

Lee, M. W., D. R. Hutchinson, T. S. Collett, and W. P. Dillon, Seismic velocities for hydrate bearing sediments using weighted equation, *J. Geophys. Res.*, *101*, 20,347–20,358, 1996.

Majorowicz, J. A., and S. L. Smith, Review of ground temperatures in the Mallik field area: A constraint to the methane hydrate stability, in *Scientific Results from JAPEX/JNOC/GSC Mallik 2L-38 Gas Hydrate Research Well, Mackenzie Delta, Northwest Territories, Canada*, edited by S. R. Dallimore, T. Uchida, and T. S. Collett, *Bull. Geol. Surv. Can.*, *544*, 45–56, 1999.

Murphy, W. F., Massilon sandstone and Vycor porous glass, *J. Acoust. Soc. Am.*, *71*, 1458–1468, 1982.

Ohara, T., S. R. Dallimore, and E. Fercho, Drilling operations, JAPEX/JNOC/GSC Mallik 2L-38 gas hydrate research well, in *Scientific Results from JAPEX/JNOC/GSC Mallik 2L-38 Gas Hydrate Research Well, Mackenzie Delta, Northwest Territories, Canada*, edited by S. R. Dallimore, T. Uchida, and T. S. Collett, *Bull. Geol. Surv. Can.*, *544*, 19–30, 1999.

Paillet, F. L., and C. H. Cheng, *Acoustic Waves in Boreholes*, CRC Press, Boca Raton, Fla., 1991.

Pearson, C. F., P. M. Halleck, P. L. McGuire, R. Hermes, and M. Mathews, Natural gas hydrates deposits: A review of in situ properties, *J. Phys. Chem.*, *87*, 4180–4185, 1983.

Sakai, A., Velocity analysis of vertical seismic profile (VSP) survey at JAPEX/JNOC/GSC Mallik 2L-38 gas hydrate research well, and related problems for estimating gas hydrate concentration, in *Scientific Results*

from JAPEX/JNOC/GSC Mallik 2L-38 Gas Hydrate Research Well, Mackenzie Delta, Northwest Territories, Canada, edited by S. R. Dallimore, T. Uchida, and T. S. Collett, *Bull. Geol. Surv. Can.*, *544*, 323–340, 1999.

Sloan, E. D., *Clathrate Hydrates of Natural Gases*, Marcel Dekker, New York, 1990.

Sun, X., X. Tang, C. H. Cheng, and L. N. Frazer, *P*- and *S*-wave attenuation logs from monopole sonic data, *Geophysics*, *65*, 755–765, 2000.

Tsang, L., and D. Rader, Numerical evaluation of transient acoustic waveforms due to a point source in a fluid-filled borehole, *Geophysics*, *44*, 1706–1720, 1979.

Uchida, T., R. Matsumoto, A. Waseda, T. Okui, K. Yamada, T. Uchida, S. Okada, and O. Takano, Summary of physicochemical properties of natural gas hydrate and associated gas-hydrate-bearing sediments, JAPEX/JNOC/GSC Mallik 2L-38 gas hydrate research well, by the Japanese research consortium, in *Scientific Results from JAPEX/JNOC/GSC Mallik 2L-38 Gas Hydrate Research Well, Mackenzie Delta, Northwest Territories, Canada*, edited by S. R. Dallimore, T. Uchida, and T. S. Collett, *Bull. Geol. Surv. Can.*, *544*, 205–228, 1999.

Walia, R., Y. Mi, R. D. Hyndman, and A. Sakai, Vertical seismic profile (VSP) in the JAPEX/JNOC/GSC Mallik 2L-38 gas hydrate research well, in *Scientific Results from JAPEX/JNOC/GSC Mallik 2L-38 Gas Hydrate Research Well, Mackenzie Delta, Northwest territories, Canada*, edited by S. R. Dallimore, T. Uchida, and T. S. Collett, *Geol. Surv. Can. Bull.*, *544*, 323–340, 1999.

Wood, A. B., *A Textbook of Sound*, G. Bell, London, 1941.

Wood, W. T., and C. Ruppel, Seismic and thermal investigations of the Blake Ridge gas hydrate area: A synthesis, *Proc. Ocean Drill. Program, Sci. Results*, *164*, 253–264, 2000.

Wood, W. T., W. S. Holbrook, and H. Hoskins, In situ measurements of *P*-wave attenuation in the methane hydrate- and gas-bearing sediments of the Blake Ridge, *Proc. Ocean Drill. Program, Sci. Results*, *164*, 265–272, 2000.

Wright, J. F., A. E. Taylor, S. R. Dallimore, and F. M. Nixon, Estimating in situ gas hydrate saturation from core temperature observations, JAPEX/JNOC/GSC Mallik 2L-38 gas hydrate research well, in *Scientific Results from JAPEX/JNOC/GSC Mallik 2L-38 Gas Hydrate Research Well, Mackenzie Delta, Northwest Territories, Canada*, edited by S. R. Dallimore, T. Uchida, and T. S. Collett, *Bull. Geol. Surv. Can.*, *544*, 101–108, 1999.

Xu, W., and C. Ruppel, Predicting the occurrence, distribution, and evolution of methane gas hydrate in porous marine sediments, *J. Geophys. Res.*, *104*, 5081–5095, 1999.

D. Goldberg and G. Guerin, Borehole Research Group, Lamont-Doherty Earth Observatory, Route 9W, Palisades, NY 10964, USA. (goldberg@ldeo.columbia.edu; guerin@ldeo.columbia.edu)